



# Antibacterial forsterite ( $\text{Mg}_2\text{SiO}_4$ ) scaffold: A promising bioceramic for load bearing applications



Rajan Choudhary<sup>a</sup>, Ankita Chatterjee<sup>b</sup>, Senthil Kumar Venkatraman<sup>a</sup>, Sivasankar Koppala<sup>c</sup>, Jayanthi Abraham<sup>b</sup>, Sasikumar Swamiappan<sup>a,\*</sup>

<sup>a</sup> Department of Chemistry, School of Advanced Sciences, VIT University, Vellore, 632014, Tamil Nadu, India

<sup>b</sup> Microbial Biotechnology Laboratory, School of Biosciences and Technology, VIT University, Vellore, 632014, Tamil Nadu, India

<sup>c</sup> Faculty of Metallurgical and Energy Engineering, Kunming University of Science and Technology, Kunming, 650093, Yunnan Province, PR China

## ARTICLE INFO

### Article history:

Received 24 October 2017

Received in revised form

12 February 2018

Accepted 24 March 2018

Available online 3 April 2018

### Keywords:

Magnesium silicate

Bone

Antibacterial

Dissolution

Mechanical stability

## ABSTRACT

In the current work, forsterite samples with different surface area were investigated for its antibacterial activity. Dissolution studies show that the lower degradation of forsterite compared to other silicate bioceramics, which is a desirable property for repairing bone defects. Forsterite scaffold shows superior compressive strength than the cortical bone after immersion in simulated body fluid. Bactericidal tests indicate that the forsterite had inhibition effect on the growth of clinical bacterial isolates. Forsterite may be a suitable candidate material for load bearing applications with enhanced mechanical properties and lower degradation rate.

© 2018 The Authors. Production and hosting by Elsevier B.V. on behalf of KeAi Communications Co., Ltd. This is an open access article under the CC BY-NC-ND license (<http://creativecommons.org/licenses/by-nc-nd/4.0/>).

## 1. Introduction

During the last 10 years, a new class of surface active bioceramics comprising of bioactive silicates have been explored as suitable candidates for hard tissue regeneration. Wollastonite ( $\text{CaSiO}_3$ ), larnite ( $\text{Ca}_2\text{SiO}_4$ ), diopside ( $\text{CaMgSi}_2\text{O}_6$ ), akermanite ( $\text{Ca}_2\text{MgSi}_2\text{O}_7$ ), bredigite ( $\text{Ca}_7\text{MgSi}_4\text{O}_{16}$ ) etc., are the few silicates which are known for their bioactivity [1–5]. However, more scientific research is needed to predict the use of bioactive silicates for load/stress bearing prosthesis. Forsterite ( $\text{Mg}_2\text{SiO}_4$ ) is an alternative bioceramic with superior mechanical properties when compared to hydroxyapatite and bioglass [6–9].

Forsterite possesses slow hydroxyapatite (HAp) deposition ability and stimulates proliferation and adhesion of osteoblast cells [6,7]. These findings indicate that forsterite can be a good choice for tissue engineering. Naturally occurring forsterite is often associated with its binary oxides including periclase (MgO), enstatite ( $\text{MgSiO}_3$ ) etc. Therefore, different synthetic procedures such as polymer

matrix method, microwave sintering, sol-gel method, auto-combustion etc. used for the preparation of pure forsterite [10–13]. Generally, the phase purity of forsterite achieved at higher temperature due to slow diffusion rate of magnesium silicate systems [14]. These challenges avoided by ball milling and compacting the precursors or by adopting mechanical activation during its synthesis [7].

The bacterial adhesion on biomaterial surface is indicated as the initial stage of bacterial contaminations leading to biofilm formation [15]. After this stage, the pathogens become resistant to antibiotics and cannot be completely removed by antimicrobial agents [16]. The expensive treatment involving systematic administration of antibiotics causes severe problems in liver and kidneys and antibiotic-resistant bacterial strains often cause implant failure leading to multiple surgeries [17]. Earlier findings suggest that bioactive glass possesses reasonable antibacterial activity than pure hydroxyapatite [18–21]. The hydroxyapatite doped with copper and zinc has been prepared to examine their antimicrobial activity [22]. Studies also reveal that the accretion of metallic ions causes cytotoxicity in bone by affecting their biocompatibility [23]. Hence, the best remedy to avoid such bacterial contaminations in implants is by developing biomaterials with intrinsic antibacterial activity.

In the present report, sol-gel combustion derived forsterite

\* Corresponding author.

E-mail address: [ssasikumar@vit.ac.in](mailto:ssasikumar@vit.ac.in) (S. Swamiappan).

Peer review under responsibility of KeAi Communications Co., Ltd.

ceramic powder was made as scaffolds. The purpose of current work is to analyze the mechanical behavior of forsterite samples synthesized by sol-gel combustion method by using different fuels. Due to the change of fuels for synthesizing material, the properties associated with the material can be altered. The degradation characteristics of the forsterite scaffolds studied by immersing it in the simulated body fluid (SBF) and mechanical tests performed on the scaffolds, after removing from the SBF Solution. A detailed study was performed for different biofilm-forming bacteria to understand the mechanism involved in the antibacterial activity of magnesium silicate bioceramics.

## 2. Experimental procedure

Forsterite powders prepared by sol-gel combustion method using glycine (FG) and urea (FU) as fuels. Briefly, the stoichiometric concentration of magnesium nitrate (99.0% SDFCL), Tetraethyl Ortho Silicate (98%, Acros Organics) and glycine (99.5% SDFCL) mixed in a beaker and stirred. In a separate beaker all the starting materials ( $\text{Mg}(\text{NO}_3)_2$ , TEOS) were mixed and in spite of glycine, urea (99% HIMEDIA) was added. Later, the pH of the reaction mixtures adjusted to 1.7 using conc. nitric acid (69–72%, SDFCL) as a catalyst. This step accelerates the rate of hydrolysis and polycondensation reactions leading to the formation of long polymeric chains in the form of a gel. The gel containing beakers were aged at room temperature for 2–3 days and dried at 70 °C in a hot air oven. The dried gels decomposed separately in a pre-heated muffle furnace at 400 °C for 30 min and finally, the combusted precursor calcined at different temperatures to optimize their phase purity. The pure forsterite samples obtained after calcination at 900 °C (FG) and 1100 °C (FU) was characterized by SEM/EDX prior to antibacterial studies. The forsterite samples were characterized by BET to analyze their surface area. To perform the SEM/EDX for the samples before and after antibacterial studies, the samples were washed in a series of ethanol: 10 min in 70%, 10 min in 95% and 20 min in 100%. The ethanol-washed samples were air-dried and dehydrated. The samples were then mounted on the stubs with adhesive carbon tapes and coated with gold in a sputter coater. The samples were analyzed under high vacuum at 10 kV. The samples (FG and FU) were sintered at 1300 °C for 3 h to study degradation and mechanical stability. Prior to these studies, the purity of the samples was analyzed by XRD.

### 2.1. Characterization

Phase evolution of sintered forsterite scaffolds was examined by X-Ray Diffractometer (Bruker, D8 advance, Germany), using Cu K $\alpha$ , Ni-filtered radiation. The maximum angular accuracy allowed in XRD for 2 $\theta$  deviation is  $\pm 0.01^\circ$ . Scanning electron microscopy (SEM-CARL ZEISS) was used to analyze the surface morphology and Energy dispersive X-ray spectroscopy (EDX- OXFORD Inc.) was used to study elemental composition of forsterite. Brunauer-Emmett-Teller (BET) method with nitrogen gas adsorption was employed for the measurement of surface area. The equipment was gas sorption system Autosorb iQ and ASiQWin Version 5 model 6 analyser from Quantachrome. Samples were degassed at 150 °C for 12 h in the presence of helium to remove physically absorbed moisture prior to BET measurements.

### 2.2. Degradation studies

The degradation behavior of FG and FU samples was performed for 30 days to examine the weight change by immersing in SBF. The SBF solution was prepared according to Kokubo's protocol [24]. Forsterite (FU and FG) was molded into cylindrical scaffolds (13 mm

diameter  $\times$  6.5 mm height) and sintered at 1300 °C at a rate of 5 °C min for 3 h. The samples were cooled to room temperature, immersed in a static SBF and incubated at 37 °C  $\pm$  0.3. The initial weight of scaffolds before immersion was accurately measured by using weighing balance. After one month, the scaffolds taken out from SBF were dried at 150 °C for a day and then the final weight was measured. The test was repeated three times for each scaffold ( $n = 3$ ) and the weight loss from the scaffold was expressed in terms of percentage (%) based on its initial weight [25].

### 2.3. Mechanical properties

The procedure followed for the preparation of forsterite scaffolds for mechanical studies was as per ASTM specifications discussed elsewhere [4]. The forsterite scaffolds obtained after degradation analysis were examined for mechanical stability using the universal testing machine (UTM) INSTRON 8801. The forsterite scaffolds were tested at an extension rate of 0.6 mm and compression rate of 1 mm/min. The test was repeated three times for each scaffold ( $n = 3$ ) and the data is presented as the mean with standard deviation.

### 2.4. Antibacterial assay

The efficiency of forsterite samples (FG and FU) against nine clinical pathogenic bacteria's (*Staphylococcus aureus*, *Enterococcus species*, *Escherichia coli*, *Serratia marcescens*, *Pseudomonas aeruginosa*, *Klebsiella pneumoniae*, *Salmonella species*, *Shigella species*, and *Proteus mirabilis*) was studied. *Staphylococcus aureus* is the predominant bacterium that infects orthopedic infection in implants and inflammation of joints and bones resulting in septic arthritis and osteomyelitis [26,27]. Another Gram positive organism, *Enterococcus sp.* is associated with chronic osteomyelitis [28]. Among Gram negative bacteria, *Pseudomonas aeruginosa* has been reported to play a role in causing postoperative orthopedic operations [29]. *Escherichia coli*, being able to beta-lactamase, have been associated with joint and bone infections and has been demonstrated in various studies [30]. Acute hematogenous osteomyelitis is the most common type of osteomyelitis which is caused by *Escherichia coli*, *Pseudomonas aeruginosa* and *Salmonella sp.* since ages [31]. In few cases, osteomyelitis along with soft tissue infection has also been recorded to cause by *Klebsiella pneumoniae* [32]. *Serratia marcescens* is well known for causing nosocomial infections and has been noted to cause both osteomyelitis and septic arthritis in immunocompetent individuals [33]. Moreover, *Staphylococcus aureus*, *Escherichia coli*, *Salmonella sp.*, *Shigella sp.*, and *Pseudomonas aeruginosa* are also responsible for causing hip joint infections [34]. Along with these organisms, *Proteus mirabilis* has also been isolate from patients suffering from hip prosthesis infection around the implants post hip replacement surgery [35]. The prevention of these bacterial infections is considered as a major concern in the biomedical field. Hence, to check the activity of forsterite samples, these clinical pathogens were used.

Broth dilution technique was chosen to determine the antibacterial activity of the forsterite samples. The forsterite being insoluble in most of the organic solvents, their diffusion capability in agar is limited, hence, broth dilution method was chosen with various concentrations of forsterite samples. The pathogenic bacterial strains were suspended in Luria-Bertani broth in presence of different concentrations (0.5, 1 and 2 mg/mL) of forsterite [36]. The concentrations were obtained by adding 0.5 mg, 1 mg and 2 mg of the forsterite per 1 ml of broth respectively. The broth containing the pathogens and forsterite was incubated under shaking condition for 24 h and the bacterial growth was determined by observing the optical density by ELISA reader (Biotek-elx800). Bacterial

growth without forsterite sample was used as a control which was compared with the forsterite containing bacterial suspension to evaluate the percentage of inhibition [37]. Dilutions of control and test broth medium were plated on Mueller-Hinton agar plates to check the colony formation and verify the bactericidal activity of

the compounds by evaluating the numbers of colonies appearing on the agar plates. The inhibitory effect of the forsterite against clinical pathogens were checked thrice ( $n = 3$ ) and thus the results obtained from the test were represented as the mean with standard deviation.

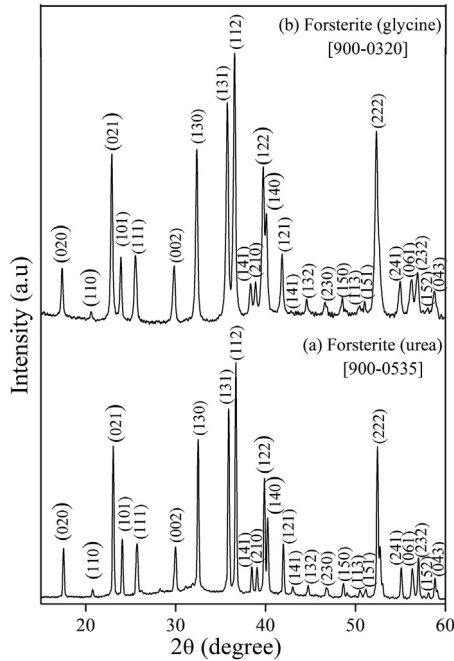


Fig. 1. XRD pattern of forsterite samples after sintering.

### 3. Results and discussion

#### 3.1. XRD analysis of forsterite

The XRD pattern of forsterite scaffolds (FG and FU) after sintering is shown in Fig. 1. The pattern shows the presence of highly crystalline characteristic peaks associated with forsterite. Both the forsterite scaffolds were matched with the standard JCPDS data card and indexed. This analysis indicates that both the scaffolds obtained after sintering were composed of forsterite.

#### 3.2. Surface and elemental analysis

The surface morphology of forsterite samples was analyzed by SEM and it is shown in Fig. 2. The surface of FG and FU shows the presence of small aggregated particles having flake-like morphology (Fig. 2a–c). The EDX analysis (Fig. 2b–d) shows the presence of all essential elements to satisfy the chemical composition of forsterite (Mg, Si, and O).

#### 3.3. BET analysis

The BET results showed that the surface area of FG was  $13.42 \text{ m}^2/\text{g}$  whereas FU possess  $3.1 \text{ m}^2/\text{g}$ . The surface area of forsterite prepared by using glycine as a fuel was found to be 4 times greater than urea. It reveals that choice of fuel has significant

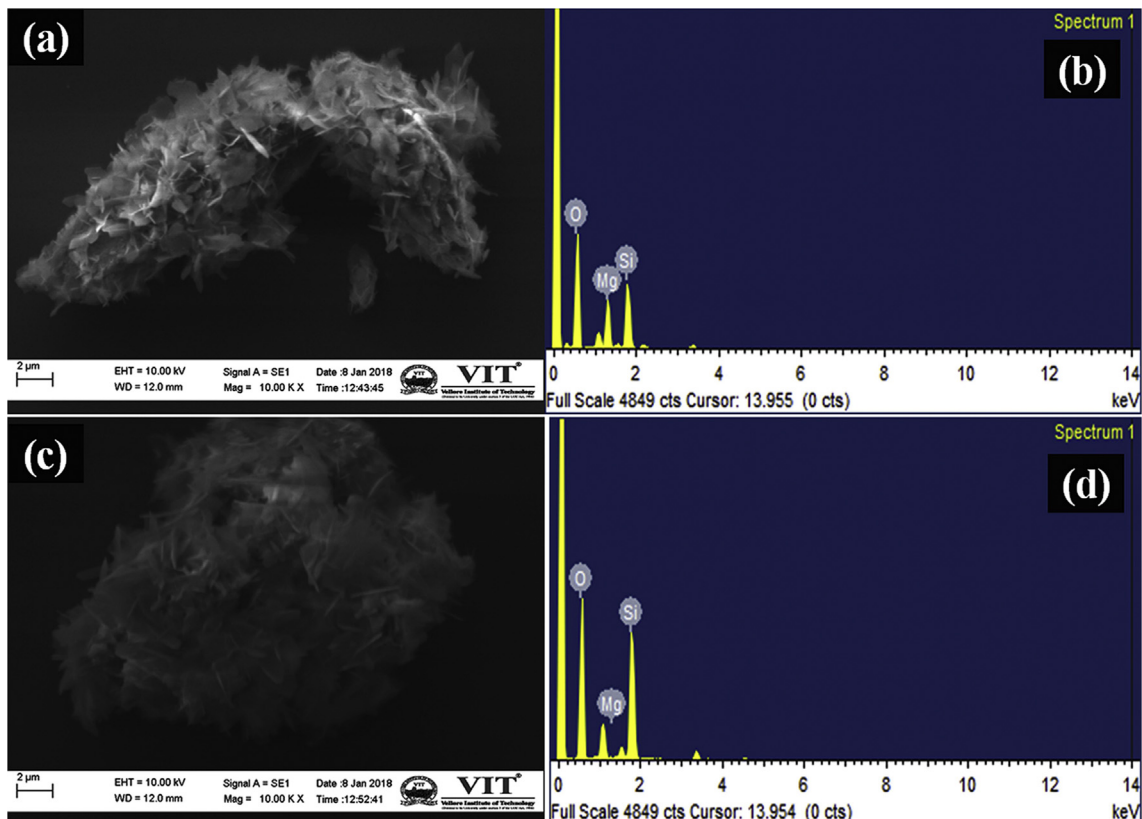


Fig. 2. SEM micrographs of FG (a), FU (c) and EDX pattern of FG (b), FU (d) samples.

impact on the surface area of the samples. Hence, selection of an appropriate fuel determines the surface area of the final product.

### 3.4. Degradation evaluation

The degradation of FG and FU scaffolds examined after immersion in SBF solution for 30 days are shown in Fig. 3a. The weight loss from FG (2.8%) was noticeably greater than that of FU (0.78%) scaffold. About 3% weight loss from the forsterite ceramic was detected when immersed in Ringer's solution while 1.2% was noticed after immersion of forsterite samples in Tris-HCl without refreshing the medium [38,39]. Although the medium used in current work to study degradation behavior was different, the weight loss from FG and FU scaffolds was quite similar to these reports. The degradation rate of FG and FU scaffolds are different due to the variation in their surface area. Wei et al. (2008) suggested that nanomaterials exhibit faster degradation rate than micron-sized owing to their small size and huge specific surface area [40].

### 3.5. Mechanical testing

The FG and FU scaffolds show variations in their compressive strength and Young's modulus which is shown in Fig. 3b–c. The fuels used in the preparation of forsterite have a significant effect on the mechanical properties of the forsterite scaffolds. FG shows a compressive strength of 201 MPa and Young's modulus of 4.8 GPa. The compressive strength and Young's modulus of FU were found to be 124 MPa and 4.6 GPa respectively. The forsterite scaffold prepared using glycine as a fuel (FG) has 1.5 times greater compressive strength than FU while Young's modulus of FG and FU were found to be almost same.

The influence of particle size on the mechanical strength of wollastonite was studied and observed that fine powders (6  $\mu\text{m}$ ) have more mechanical stability than coarse powders (44  $\mu\text{m}$ ) by about 50% [41]. It was also observed that the increase in particle size resulted in a decrease in mechanical strength [42]. Thus, the potential reason for the difference in mechanical properties is due to the change in particle size based on the fuel used. Forsterite

prepared by using glycine as a fuel shows high surface area whereas in case of forsterite prepared by using urea as fuel exhibits less surface area. Narayan (2009) emphasized that during sintering the final pore size and their distribution will be determined by the characteristics of the starting powder: smaller the particle size, smaller will be the pores between adjacent particles that will result in better mechanical strength of the material [43].

Other silicate bioceramics such as diopside and Mg-substituted wollastonite show a decrease in mechanical strength after degradation studies [44,45]. About, 2% weight loss was found in diopside after four weeks of immersion in SBF and decrease in compressive strength (1.36–0.20 MPa) and compressive modulus (68–10 MPa) was observed. The Mg-substituted wollastonite reveals a decrease in compressive strength from 37 MPa to 29 MPa after 8 weeks of immersion in tris buffer. The main reason for such behavior is that during immersion studies dissolution of the bioceramic may result in weight loss, strength and apatite deposition leads to increase in mechanical property [45]. Hence, any one of these mechanisms occurring dominantly will determine the final weight change and strength. That is why wollastonite and diopside show a decrease in mechanical properties. The results observed in the current study reveal that the forsterite scaffolds possess good mechanical stability even after immersion in SBF for 30 days as compared to existing reports.

Table 1 shows compressive strength and Young's modulus values of cancellous and cortical bone [46]. In current work, both FG

**Table 1**  
Mechanical properties of bone and their comparison with forsterite bioceramics.

Samples	Mechanical Properties		
	Compressive strength (MPa)	Young's modulus (GPa)	
Cancellous Bone [46]	0.1–16	0.05–0.5	
Cortical Bone [46]	130–200	7–30	
Forsterite	FU	124 $\pm$ 9.0	4.6 $\pm$ 0.1
	FG	201 $\pm$ 15	4.8 $\pm$ 0.1

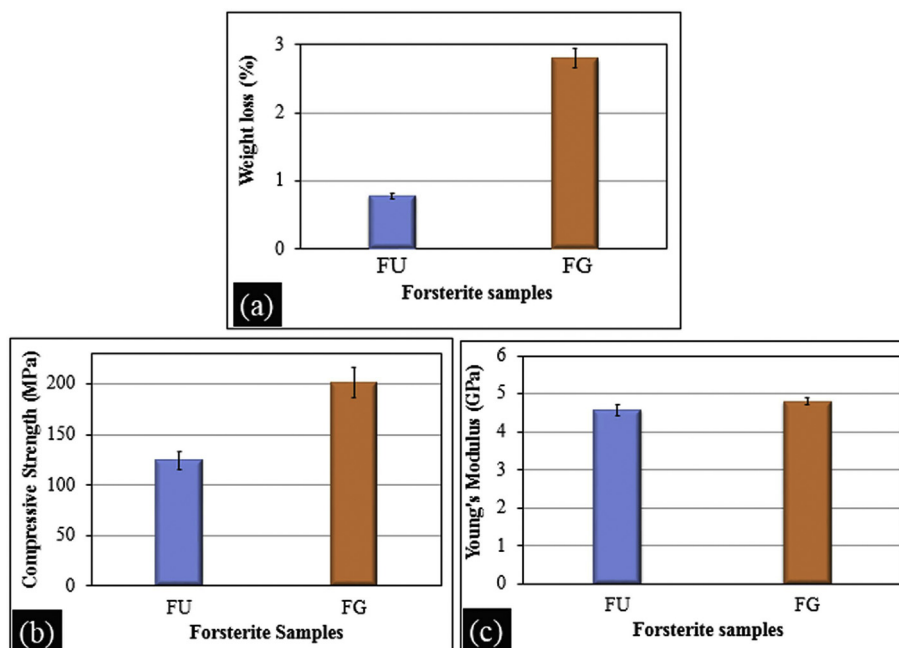


**Fig. 3.** Degradation behavior (a) compressive strength (b) and Young's modulus (c) of forsterite samples after 30 days of immersion in SBF.

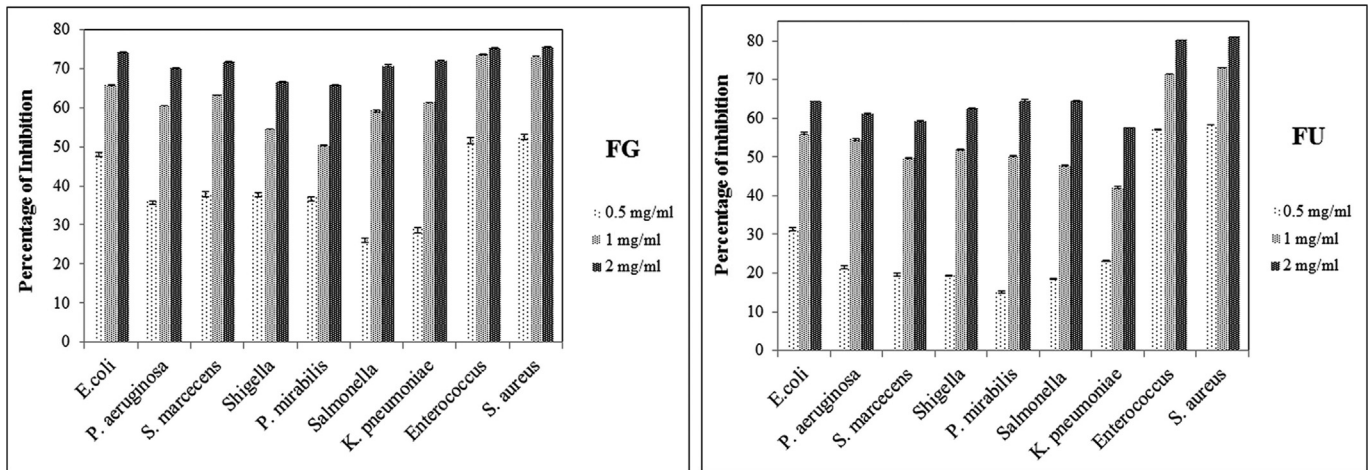


Fig. 4. Percentage inhibition of different clinical pathogens by pure forsterite (FG and FU).

and FU scaffolds have superior compressive strength than that of cancellous bone. In comparison to cortical bone, FG possesses higher value while FU seems to be close to the lower limit of cortical bone. The Young's modulus noticed for FG and FU scaffolds is quite higher than cancellous bone but inferior to that of the cortical bone. These observations indicate that forsterite possesses good mechanical property and can be used for load-bearing applications or as a composite material to enhance the mechanical properties of the calcium silicates and polymers used in biomedical applications.

### 3.6. Antibacterial activity

The antibacterial activity of forsterite against Gram-positive and Gram-negative bacteria is shown in Fig. 4. The experimental trials were followed thrice and the results obtained were calculated as mean and were found to be statistically significant. The difference in the cellular makeup of Gram-positive and Gram-negative led to variations in their inhibition activity. Thus, forsterite observed to be more effective against Gram-positive bacteria, such as *Staphylococcus aureus* and *Enterococcus species*. At 2 mg/mL, FG and FU could inhibit  $75.6 \pm 0.1$  and  $81 \pm 0.04\%$  of *Staphylococcus aureus* respectively. Among the Gram-negative bacterial isolates, FG showed the highest inhibitory effect on *Escherichia coli* followed by *Klebsiella pneumoniae*, *Serratia marcescens*, *Salmonella species*, *Pseudomonas aeruginosa*, *Shigella species* and *Proteus mirabilis*. In the case of FU, the highest rate of growth inhibition observed in *Proteus mirabilis*. The comparative study of the forsterite samples reveals FG has more potent on Gram-negative bacteria than FU, whereas, the Gram-positive organisms inhibited at a higher rate by the FU when compared to FG. The percentage inhibition of the

clinical pathogens by forsterite samples are shown in Table 2.

A change in pH observed during the antibacterial study of forsterite. The pH of the broth was found to increase from 6.8 in the initial stage to 7.5 by the end of 24 h incubation period. The increasing pH of the media was found to have a correlation with the bactericidal activity of the forsterite. The pH of the broth found to increase, which played a role in the decrease of microbial concentration in the broth. The magnesium ions in forsterite after dissolution increases the pH and turns the broth to basic. The magnesium being alkaline in nature imparts a strong antibacterial activity [47]. The pH of the broth at the beginning of the experiment was 6.8, which increased to 7.5 by the end of 24 h incubation as shown in Table 3 and Table 4. The increasing pH of the media was found to have a correlation with the bactericidal activity of the forsterite. The rise in the pH of broth creates disability in the bacterial cells, thus inhibiting the growth of microorganisms. The alkaline ions react with the protons and forms hydroxyl ions, which result in high pH and thus kill the bacteria [48].

The growth of *S. aureus* and *E. coli* on Mueller Hinton agar medium was compared between control and forsterite samples to examine the colony formation (Fig. 5). It is evident that all the FG and FU have the ability to prevent bacterial growth at 2 mg/mL concentration. The growth of bacterial colonies in agar medium

Table 3  
Changes in pH after 24 h incubation for *Escherichia coli*.

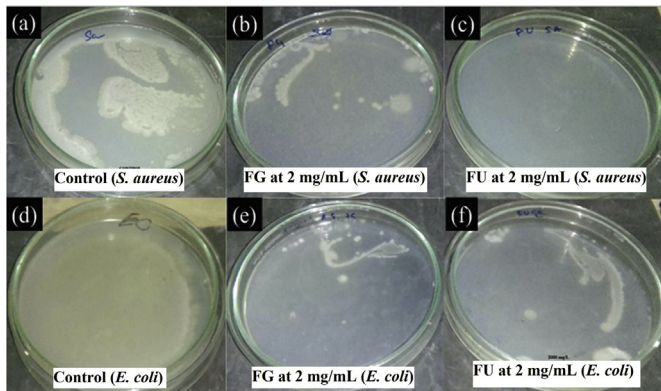
Samples	Control	0.5 mg/mL	1 mg/mL	2 mg/mL
FG	6.8	7	7.2	7.5
FU	6.8	7	7.1	7.3

Table 2  
Percentage inhibition of the clinical pathogens by FG and FU.

Pathogens	Percentage of Inhibition by FG			Percentage of Inhibition by FU			
	Concentrations (mg/mL)			Concentrations (mg/mL)			
	0.5	1	2	0.5	1	2	
GRAM NEGATIVE STRAINS	<i>Escherichia coli</i>	48.4 ± 0.1	65.9 ± 0.1	74.2 ± 0.1	31.3 ± 0.4	56.1 ± 0.2	64.3 ± 0.1
	<i>Pseudomonas aeruginosa</i>	36.2 ± 0.04	60.4	70.1 ± 0.2	21.6 ± 0.4	54.6 ± 0.3	61.3 ± 0.1
	<i>Serratia marcescens</i>	38.3 ± 0.3	63.3	71.7 ± 0.2	19.5 ± 0.4	49.8 ± 0.1	59.2 ± 0.1
	<i>Shigella sp.</i>	38.1 ± 0.1	54.4 ± 0.1	66.6 ± 0.1	19.3 ± 0.1	51.9 ± 0.1	62.6 ± 0.1
	<i>Proteus mirabilis</i>	37 ± 0.1	50.3 ± 0.1	65.7 ± 0.1	15.1 ± 0.2	50.3 ± 0.1	64.6 ± 0.2
	<i>Salmonella sp.</i>	26.4 ± 0.1	59.1 ± 0.2	70.7 ± 0.2	18.5 ± 0.1	47.8 ± 0.1	64.4 ± 0.1
	<i>Klebsiella pneumoniae</i>	29 ± 0.2	61.3 ± 0.1	72.0 ± 0.1	23.1 ± 0.1	42.1 ± 0.2	57.5 ± 0.1
GRAM POSITIVE STRAINS	<i>Enterococcus sp.</i>	51.6 ± 0.4	73.7 ± 0.2	75.1 ± 0.1	57.1 ± 0.04	71.4 ± 0.04	80.2 ± 0.04
	<i>Staphylococcus aureus</i>	52.8 ± 0.2	73.9 ± 0.1	75.6 ± 0.1	58.3 ± 0.1	73.1 ± 0.04	81 ± 0.04

**Table 4**  
Changes in pH after 24 h incubation for *Staphylococcus aureus*.

Samples	Control	0.5 mg/mL	1 mg/mL	2 mg/mL
FG	6.8	7.1	7.2	7.4
FU	6.8	7	7.2	7.3



**Fig. 5.** Growth of *S. aureus* on (a) control, (b) FG 2 mg/mL, (c) FU 2 mg/mL; The growth of *E. coli* on (d) control, (e) FG 2 mg/mL and (f) FU 2 mg/mL in agar medium.

concluded that FU has the ability to inhibit the growth of *S. aureus* (Fig. 5c) more than that of *E. coli* (Fig. 5f) while FG shows similar inhibition behavior against both *E. coli* and *S. aureus* (Fig. 5b–e). This data reveals that forsterite samples have potential to arrest the bacterial growth at a concentration of 2 mg/mL.

Recently, Saqaei et al. (2016) reported the antibacterial activity of 58S bioactive glass-forsterite nanocomposite powders [49]. The report suggests that the pure forsterite nanopowders were unable to inhibit the bacterial growth at the concentrations ranging from 25 to 200 mg/mL. Moreover, the nanocomposites showed an

intense antibacterial activity above 50 mg/ml concentration. Whereas in this study, the forsterite samples have shown bactericidal activity at a very low concentration (2 mg/mL). These results found to be quiet superior to the previous reports where the ceramics particles showed bactericidal activity at 50 mg/mL [18,48]. The sol-gel combustion derived forsterite explored as a new bactericidal material in this study.

The overall bactericidal activity of FG was greater than that of FU due to the variation in surface area of the particles prepared. Surface area of the FG samples is found to be 4 times higher than the FU samples hence FG shows better antibacterial activity. The nanoparticles have a high surface area, which promotes the faster ionic release and greater reactivity. The previous report states that nanopowders have a higher level of solubility and faster release of calcium, silicate and phosphorus ions resulting into an increase in pH of the medium [19]. Hence, the pH level of FG culture medium was noticed to be higher than FU during antibacterial studies as shown in Tables 3 and 4.

The mechanism behind the antibacterial activity of forsterite may be due to the increase in pH of the culture medium. Since, the change in pH was found to be hostile to bacterial growth [18,20]. Moreover, bacteria are usually 1–3  $\mu\text{m}$  in length. Therefore, nanoparticles may cluster around the bacteria cell to deactivate the membrane proteins, and destabilize the bacterial membrane resulting in the death of bacteria by leaking of genetic material, proteins, and minerals from the disrupted cell wall [50]. The clustering of the forsterite particles around the clinical pathogens has been noticed under scanning electron microscopy (Fig. 6). The control images of *E. coli* and *S. aureus* shows the smoothly surfaced cells (Fig. 6a and d) whereas post-experimental trials with forsterite, the cells were covered by the clusters of the particles (Fig. 6b–c and Fig. 6e–f). Hence, chemical composition, surface area and concentration of bioactive silicates in the culture medium might be the factors to confirm antibacterial property.

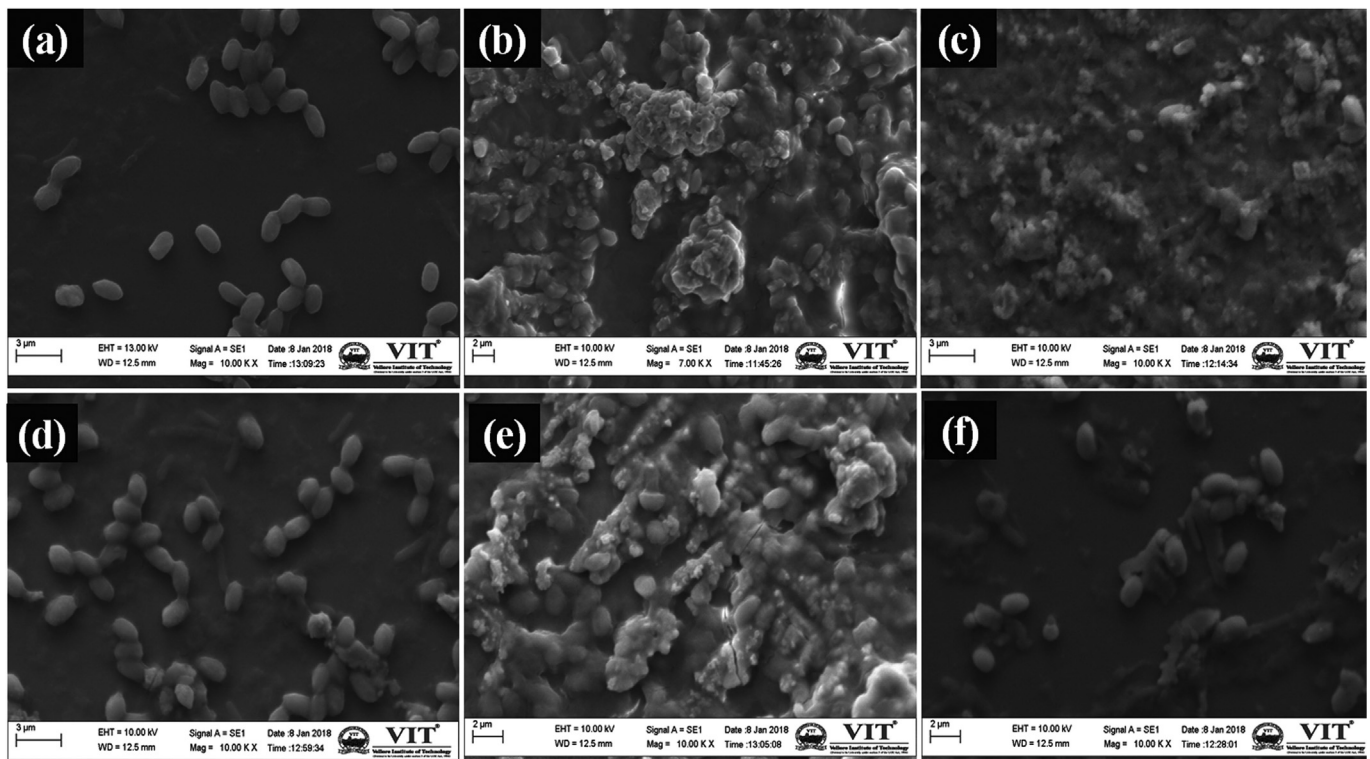


**Fig. 6.** SEM micrographs of forsterite samples after antibacterial studies; Control *E. coli* (a), FG *E. coli* (b), FU *E. coli* (c), Control *S. aureus* (d), FG *S. aureus* (e), FU *S. aureus* (f).

#### 4. Conclusion

Forsterite with high surface area possess better degradability, mechanical strength and antibacterial activity. The mechanical properties of forsterite are found to be equivalent to that of the cortical bone even after 30 days of immersion in SBF. Forsterite samples have remarkable bactericidal activity against bacterial pathogens at a very low concentration than those utilized for clinical applications. The change in pH was found to be the major reason for the bactericidal activity of forsterite. Thus, forsterite can be utilized as a potential material for load bearing applications or an antibacterial ceramic for biocoatings.

#### Acknowledgment

This research was financially supported by Vellore Institute of Technology Research Grants for Engineering, Management, and Science (VITRGEMS). The authors thank DST-FIST for the XRD and SEM/EDX characterization. Also thankful to CAMPT-VIT for Mechanical testing.

#### References

- [1] T. Kitsugi, T. Nakamura, T. Yamamura, T. Kokubu, T. Shibuya, M. Takagi, SEM-EPMA observation of three types of apatite containing glass-ceramics implanted in bone: the variance of a Ca-P-rich layer, *J. Biomed. Mater. Res.* 21 (1987) 1255–1271.
- [2] M. Nakano, Implant study of glass-ceramics in rat femurs—evaluations for dental implant applications, *The Journal of the Stomatological Society* 58 (1991) 198–233.
- [3] X. Liu, S. Tao, C. Ding, Bioactivity of plasma sprayed dicalcium silicate coatings, *Biomaterials* 23 (2002) 963–968.
- [4] C. Wu, J. Chang, Synthesis and apatite-formation ability of akermanite, *Mater. Lett.* 58 (2004) 2415–2417.
- [5] C. Wu, J. Chang, J. Wang, S. Ni, W. Zhai, Preparation and characteristics of a calcium magnesium silicate (bredigite) bioactive ceramic, *Biomaterials* 26 (2005) 2925–2931.
- [6] M. Kharaziha, M.H. Fathi, Improvement of mechanical properties and biocompatibility of forsterite bioceramic addressed to bone tissue engineering materials, *J. Mech. Behav. Biomed. Mater.* 3 (2010) 530–537.
- [7] S. Ramesh, A. Yaghoubi, K.Y. Sara Lee, K.M. Christopher Chin, J. Purbolaksono, M. Hamdi, M.A. Hassan, Nanocrystalline forsterite for biomedical applications: synthesis, microstructure and mechanical properties, *J. Mech. Behav. Biomed. Mater.* 25 (2013) 63–69.
- [8] M.H. Fathi, M. Kharaziha, Two-step sintering of dense, nanostructural forsterite, *Mater. Lett.* 63 (2009) 1455–1458.
- [9] F. Tavangarian, R. Emadi, Nanostructure effects on the bioactivity of forsterite bioceramic, *Mater. Lett.* 65 (2011) 740–743.
- [10] A. Saberi, B. Alinejad, Z. Negahdari, F. Kazemi, A. Almasi, A novel method to low temperature synthesis of nanocrystalline forsterite, *Mater. Res. Bull.* 42 (2007) 666–673.
- [11] H.B. Bafrooei, T. Ebadzadeh, H. Majidian, Microwave synthesis and sintering of forsterite nanopowder produced by high energy ball milling, *Ceram. Int.* 40 (2014) 2869–2876.
- [12] M.A. Naghiu, M. Gorea, E. Mutch, F. Kristaly, M. Tomoaia-Cotise, Forsterite nanopowder: structural characterization and biocompatibility evaluation, *J. Mater. Sci. Technol.* 29 (2013) 628–632.
- [13] K. Mostafavi, M. Ghahari, S. Baghshahi, A.M. Arabi, Synthesis of  $Mg_2SiO_4:Eu^{3+}$  by combustion method and investigating its luminescence properties, *J. Alloy. Comp.* 555 (2013) 62–67.
- [14] A. Douy, Aqueous syntheses of forsterite ( $Mg_2SiO_4$ ) and enstatite ( $MgSiO_3$ ), *J. Sol. Gel Sci. Technol.* 24 (2002) 221–228.
- [15] F. Alam, K. Balani, Adhesion force of staphylococcus aureus on various biomaterial surfaces, *J. Mech. Behav. Biomed. Mater.* 65 (2017) 872–880.
- [16] L.G. Harris, R.G. Richards, Staphylococci and implant surfaces: a review, *Injury* 37 (2006) S3–S14.
- [17] X. Lin, S. Yang, K. Lai, H. Yang, T.J. Webster, L. Yang, Orthopedic implant biomaterials with both osteogenic and anti-infection capacities and associated in vivo evaluation methods, *Nanomedicine: Nanotechnology, Biol. Med.* 13 (2017) 123–142.
- [18] S. Hu, J. Chang, M. Liu, C. Ning, Study on antibacterial effect of 45S5 bioactive glass, *J. Mater. Sci. Mater. Med.* 20 (2009) 281–286.
- [19] V. Mortazavi, M.M. Nahrkhalaji, M.H. Fathi, S.B. Mousavi, B.N. Esfahani, Antibacterial effects of sol-gel derived bioactive glass nanoparticle on aerobic bacteria, *J. Biomed. Mater. Res. A* 94 (2010) 160–168.
- [20] O. Lepparanta, M. Vaahio, T. Peltola, D. Zhang, L. Hupa, Antibacterial effect of bioactive glasses on clinically important anaerobic bacteria in vitro, *J. Mater. Sci. Mater. Med.* 19 (2008) 547–551.
- [21] A. Rajendran, R.C. Barik, D. Natarajan, M.S. Kiran, D.K. Pattanayak, Synthesis, phase stability of hydroxyapatite–silver composite with antimicrobial activity and cytocompatibility, *Ceram. Int.* 40 (2014) 10831–10838.
- [22] V. Stanic, S. Dimitrijevic, J. Antic-Stankovic, M. Mitric, B. Jokic, I.B. Plecas, S. Raicevi, Synthesis, characterization and antimicrobial activity of copper and zinc-doped hydroxyapatite nanopowders, *Appl. Surf. Sci.* 256 (2010) 6083–6089.
- [23] A.M. El-Kady, A.F. Ali, R.A. Rizk, M.M. Ahmed, Synthesis, characterization and microbiological response of silver doped bioactive glass nanoparticles, *Ceram. Int.* 38 (2012) 177–188.
- [24] T. Kokubo, H. Takadama, How useful is SBF in predicting in vivo bone bioactivity? *Biomaterials* 27 (2006) 2907–2915.
- [25] H. Li, J. Chang, In vitro degradation of porous degradable and bioactive PHBV/wollastonite composite scaffolds, *Polym. Degrad. Stabil.* 87 (2005) 301–307.
- [26] H.V. Belt, D. Neut, W. Schenk, J.R. Horn, H.C. Mei, H.J. Busscher, Infection of orthopedic implants and the use of antibiotic-loaded bone cements: a review, *Acta Orthop. Scandia* 72 (2001) 557–571.
- [27] J.A. Wright, S.P. Nair, Interaction of *staphylococci* with bone, *Int. J. Med. Microbiol.* 300 (2010) 193–204.
- [28] H.S. Framow, Systemic antimicrobial therapy in osteomyelitis, *Semin. Plast. Surg.* 23 (2009) 90–99.
- [29] H.A. Mousa, Infection following orthopaedic implants and bone surgery, *East. Medit. Health J.* 7 (2001) 738–743.
- [30] L. Cremet, S. Corvec, P. Bemer, L. Bret, C. Lebrun, B. Lesimple, A.F. Miegerville, A. Reynaud, D. Lepelletier, N. Caroff, Orthopaedic-implant infections by *Escherichia coli*: molecular and phenotypic analysis of the causative strains, *J. Infect.* 64 (2012) 169–175.
- [31] J.A. Sanders, *Klebsiella pneumoniae* osteomyelitis: demonstration by three-phase radionuclide bone imaging, *J. Nucl. Med.* 30 (1989) 1412–1414.
- [32] C.D. Odio, D. Duin, E. Cober, L. Teixeira-Johnson, S. Schmitt, J. Sanctis, Carbapenem-resistant *Klebsiella pneumoniae* osteomyelitis and soft tissue infections: a descriptive case series, *J. Infect. Dis. Ther.* 3 (2015) 1–4.
- [33] H. Hadid, M. Usman, S. Thapa, Severe osteomyelitis and septic arthritis due to *Serratia marcescens* in an immunocompetent patient, *Case Rep. Infect. Dis.* 2015 (2015) 1–3.
- [34] U. Geipel, Pathogenic organisms in hip joint infections, *Int. J. Med. Sci.* 6 (2009) 234–240.
- [35] C.A. Aboltins, M.M. Dowsey, K.L. Buising, T.N. Peel, J.R. Daffy, P.F. Choong, P.A. Stanley, Gram-negative prosthetic joint infection treated with debridement, prosthesis retention and antibiotic regimens including a fluoroquinolone, *Clin. Microbiol. Infect.* 17 (2011) 862–867.
- [36] L. Esteban-Tejeda, C. Prado, B. Cabal, J. Sanz, R. Torrecillas, J.S. Moya, Antibacterial and antifungal activity of ZnO containing glasses, *PLoS One* 10 (2015) e0136490.
- [37] C. Valgas, S.M. Souza, E.F. Smania, A. Smania, Screening methods to determine antibacterial activity of natural products, *Braz. J. Microbiol.* 38 (2007) 369–380.
- [38] F. Tavangarian, R. Emadi, Improving degradation rate and apatite formation ability of nanostructure forsterite, *Ceram. Int.* 37 (2011) 2275–2280.
- [39] S. Ni, J. Chang, In vitro degradation, bioactivity, and cytocompatibility of calcium silicate, dimagnesium silicate, and tricalcium phosphate bioceramics, *J. Biomater. Appl.* 24 (2009) 139–158.
- [40] J. Wei, S.J. Heo, D.H. Kim, S.E. Kim, Y.T. Hyun, J.-W. Shin, Comparison of physical, chemical and cellular responses to nano- and micro-sized calcium silicate/poly( $\epsilon$ -caprolactone) bioactive composites, *J. R. Soc. Interface* 5 (2008) 617–630.
- [41] J. Lu, Z. Lu, C. Peng, X. Li, H. Jiang, Influence of particle size on sinterability, crystallisation kinetics and flexural strength of wollastonite glass-ceramics from waste glass and fly ash, *Mater. Chem. Phys.* 148 (2014) 449–456.
- [42] S. Baitalik, N. Kayal, A. Dey, O. Chakrabarti, Effect of SiC particle size on the material and mechanical properties of mullite bonded SiC ceramics processed by infiltration technique, *Ceram.—Silik* 58 (2014) 326–332.
- [43] R. Narayan, *Biomedical Materials*, Springer, USA, 2009.
- [44] C. Wu, Y. Ramaswamy, H. Zreiqat, Porous diopside ( $CaMgSi_2O_6$ ) scaffold: a promising bioactive material for bone tissue engineering, *Acta Biomater.* 6 (2010) 2237–2245.
- [45] D. He, C. Zhuang, S. Xu, X. Ke, X. Yang, L. Zhang, G. Yang, X. Chen, X. Mou, A. Liu, Z. Gou, 3D printing of Mg-substituted wollastonite reinforcing diopside porous bioceramics with enhanced mechanical and biological performances, *Bioactive materials* 1 (2016) 85–92.
- [46] L.-C. Gerhardt, A.R. Boccaccini, Bioactive glass and glass-ceramic scaffolds for bone tissue engineering, *Materials* 3 (2010) 3867–3910.
- [47] Y. Li, G. Liu, Z. Zhai, L. Liu, H. Li, K. Yang, L. Tan, P. Wan, X. Liu, Z. Ouyang, Z. Yu, T. Tang, Z. Zhu, X. Qu, K. Dai, Antibacterial properties of magnesium in vitro and in an in vivo model of implant-associated methicillin-resistant *Staphylococcus aureus* infection, *Antimicrob. Agents Chemother.* 58 (2014) 7586–7591.
- [48] S. Hu, C. Ning, Y. Zhou, L. Chen, K. Lin, J. Chang, Antibacterial activity of silicate bioceramics, *J. Wuhan Univ. Technol.-Materials Sci. Ed.* 26 (2011) 226–230.
- [49] M. Saqaei, M. Fathi, H. Edris, V. Mortazavi, N. Hosseini, Effects of adding forsterite bioceramic on in vitro activity and antibacterial properties of bioactive glass-forsterite nanocomposite powders, *Adv. Powder Technol.* 27 (2016) 1922–1932.
- [50] Q. Li, S. Mahendra, D.Y. Lyon, L. Brunet, M.V. Liga, D. Li, P.J. Alvarez, Antimicrobial nanomaterials for water disinfection and microbial control: potential applications and implications, *Water Res.* 42 (2008) 4591–4602.